

FusionMotion: Multi-Sensor Asynchronous Fusion for Continuous Occupancy Prediction via Neural-ODE

Yining Shi^{1,2}, Kun Jiang^{1*}, Ke Wang², Jiusi Li³, Yunlong Wang¹, and Diange Yang^{1*}

Abstract—Occupancy maps are widely recognized as an efficient method for facilitating robot motion planning in static environments. However, for intelligent vehicles, occupancy of both the present and future moments is required to ensure safe driving. In the automotive industry, the accurate and continuous prediction of future occupancy maps in traffic scenarios remains a formidable challenge. This paper investigates multi-sensor spatio-temporal fusion strategies for continuous occupancy prediction in a systematic manner. This paper presents FusionMotion, a novel bird’s eye view (BEV) occupancy predictor which is capable of achieving the fusion of asynchronous multi-sensor data and predicting the future occupancy map with variable time intervals and temporal horizons. Remarkably, FusionMotion features the adoption of neural ordinary differential equations on recurrent neural networks for occupancy prediction. FusionMotion learns derivatives of BEV features over temporal horizons, updates the implicit sensor’s BEV feature measurements and propagates future states for each ODE step. Extensive experiments on large-scale nuScenes and Lyft L5 datasets demonstrate that FusionMotion significantly outperforms previous methods. In addition, it outperforms the BEVFusion-style fusion strategy on the Lyft L5 dataset while reducing synchronization requirements. Codes and models will be made available.

Index Terms—Autonomous driving, Neural networks, Multi-sensor fusion, Occupancy flow prediction, Neural ordinary differential equation

I. INTRODUCTION

GRID-centric perception methods are reviving with the development of deep learning in the field of autonomous driving. Occupancy grid map (OGM) has been a long-standing requirement for robotics navigation; however, OGM has trouble adapting to large-scale dynamic traffic scenarios due to its high computation and memory requirements. In recent years, larger and more complex neural networks with increased computation demands have made possible real-time semantic dynamic occupancy networks that accurately predict semantics, occupancy, motion, and future occupancy flow.

Object-centric pipelines have been dominant components in automotive perception for a very long time, which output lists of compact object elements in 3D object detection,

tracking, and trajectory prediction pipelines. In contrast to object-centric pipelines, grid-centric perception refers back to the most fundamental spatial occupancy for a comprehensive understanding of the movement of the ego vehicle in its surrounding environment. Since static occupancy grids are insufficiently safe for highly dynamic traffic scenarios, the Dempster-Shafer theory is used to determine whether or not OGM grids are static [1]. In addition, the dynamic occupancy grid map (DOGM) is a probability-based inference method for tracking the grids’ velocities. Nuss et al. [2] propose a random finite set solution similar to particle filters and parallelization of fast inference in DOGM. Prior to deep learning, DOGMs are sensitive to particle number and susceptible to measurement noise, which hinders their use in autonomous vehicles.

Deep learning has improved the feature representation for grid mapping and motion estimation to be more precise. Two mainstream pipelines for occupancy prediction are proposed according to the sensor modalities: instance-unaware motion displacement prediction on nonempty pillars and instance-aware occupancy flow in the entire area. The fundamental issues of end-to-end occupancy prediction are the representation of spatial-temporal features from historical and current sensor data, as well as the evolution of temporal dynamics for the future. Existing pipelines typically consist of BEV grid feature representation, temporal blocks, future prediction modules, and BEV decoder. The representation of BEV characteristics is intensively discussed with respect to two topics: View projection techniques of camera-to-BEV grids; voxel feature extraction for LiDAR point clouds based on BEV. Temporal blocks are a cascade of spatial-temporal convolutional (STC) blocks with multiple scales. Future prediction modules create variants of recurrent neural networks operating on BEV feature space and provide services for short-term BEV state prediction in the future. Prior art relies on a number of assumptions that may not hold true in real-world situations. The sensor data stream is initially passed into the model at a constant frame rate. Second, the LiDAR point clouds are tightly synchronized with the images that are closest. Third, all sensors always operate normally. Fourth, in both the training and inference phases, the prediction horizons and intervals are fixedly set to be identical. In conclusion, prior arts impose stringent limitations on the uniformity of sensor data and tasks, making them inflexible for less-than-ideal conditions.

The proposed method, FusionMotion, features flexible

¹Yining Shi, Kun Jiang, Yunlong Wang, and Diange Yang are with School of Vehicle and Mobility, Tsinghua University.

{syn21, yl-wang19}@mails.tsinghua.edu.cn, {jiangkun, ydg}@mail.tsinghua.edu.cn

²Ke Wang is with DiDi Chuxing. kewang1@didiglobal.com

³Jiusi Li is with Tongji University. ljs991117@tongji.edu.cn

This work is done during Yining Shi’s internship at DiDi Chuxing.

Corresponding author: Kun Jiang, Diange Yang.

timestamp-agnostic fusion for non-uniform timestamp input, multi-sensor asynchronous fusion for spatial-temporal feature extraction, and continuous occupancy prediction by formulating temporal propagation of BEV features in a neural ordinary differential equation (N-ODE) manner. The proposed method mainly innovates the modeling of continuous change trend of implicit spatial BEV features in time series, as opposed to representing future implicit features at specific time intervals, so it realizes the function of continuous occupancy predictions on any temporal horizons and time intervals all with one single model without repeated train and test.

Our contributions are summarized as follows:

- 1) We propose a novel and robust multi-sensor asynchronous fusion perception framework, **FusionMotion**, for grid-centric perception and prediction that will not fail when a single sensor occasionally malfunctions.
- 2) We design a novel BEV feature propagation handler, **SpatialGRU-ODE**, which fuses sporadic asynchronous sensor inputs and predicts continuous occupancy flow given any time intervals and any time windows on-demand only by training the model once.
- 3) We propose a novel range-view to BEV feature representation for LiDAR pointclouds, **RV-Lift**, for better instance completion in instance-aware BEV prediction tasks.
- 4) We validate the proposed algorithm on two large-scale public automotive datasets: nuScenes and Lyft L5 datasets, and the results have demonstrated the robustness and high precision of our occupancy prediction method.

The remaining sections of this paper are structured as follows. Section II presents a brief overview of related works. FusionMotion method is elaborated in Section III. Experiments and results are analyzed and presented in Section IV. Section V concludes this paper.

II. RELATED WORKS

A. Multi-Sensor Fusion

Long-standing classifications of multi-sensor multi-modal fusion methods include data-level fusion (early-fusion), feature-level fusion (deep-fusion), and object-level fusion (late-fusion) [3], [4]. Early fusion [5], [6] relies on projection and calibration matrices to fuse raw data. Late fusion [7], [8] makes the final prediction based on the proposals in different modalities. Deep-fusion methods that fuse cross-modal data into the same feature embedding space appear to have the best representation abilities. [9]–[11] lift 2D image proposals into 3D frustums for fusion, while [12] generates 3D proposals and [13] defines 3D object queries to fuse image features.

A newly emerging trend in automotive perception is the ability to represent different modalities to the same feature embedding space, largely thanks to the rapid development of data-driven view transformation techniques of ring cameras. [14]–[16] combine multi-modal input features in a shared BEV space, whereas [17] generates 2D object queries from LiDAR BEV features to fuse image features. [18]–[20] build the voxel-based space and support feature interaction in 3D

space. Since synchronization is required for the majority of spatial fusion, we are driven to investigate a resilient and effective asynchronous fusion on BEV that does not fail given the malfunction of one modality or a single sensor.

B. Temporal Fusion

Temporal continuous information is a common and natural aggregator for perception tasks including 3D object detection, BEV segmentation, and odometry estimation in multi-view stereo settings. With regard to different modalities, LiDAR-based networks [21], [22] typically employ data-level temporal fusion, which transforms multi-frame point clouds to the current ego's coordinate as inputs via ego pose or registration methods. MPPNet [23] uses proxy points to extract long-range frame features as a solution to the issue that point cloud aggregation over longer frames creates trails on the same object.

As images cannot be transformed to the latest ego coordinate in the data level, most vision-centric methods align the BEV feature maps from multiple time steps based on ego pose, and then concatenate them for fusion [24]–[27] or support their interactions through attention [28], [29]. For query-based detectors without explicit BEV feature maps, PETRv2 [30] aligns and concatenates past and present 3D coordinates for the transformer decoder, while [31] converts previous features into a unified virtual view and employs cross-attention for long-range fusion. We leverage both data-level and feature-level wrapped-based fusion which can cope with non-uniform time interval data flow.

C. Occupancy Flow Prediction

Occupancy flow prediction, first proposed in Occupancy Flow Field [32], is a valuable supplement to trajectory-set prediction [33], [34]. Two key elements for occupancy flow prediction are future occupancy and flow vectors of each grid. The advantages of occupancy flow are a non-parametric distribution output and fine-grained grid velocity. Waymo formulates the long-range occupancy flow based on past ground-truth trajectories for its occupancy flow challenge. In contrast, end-to-end occupancy flow methods with various sensor modalities formulate the task in a different manner. Recent LiDAR-based methods [21], [22], [35] attach displacement vectors to non-empty BEV grids to describe short-term motion in future 1.0s. These networks typically have a BEV-based spatial-temporal backbone and several shared heads that indicate the classification, motion and displacement of each grid. STPN [22] and BE-STI [21] are effective BEV-based spatial-temporal feature extractors for binary-occupied grids which consist of only 2D convolutional blocks. Vision-centric pipelines usually formulate the prediction task as future instance segmentation on BEV grids. FIERY [26] is the first vision-centric stochastic future prediction method. StretchBEV [36] uses a variational autoencoder for decoupling learning of temporal dynamics and BEV decoder. Other frameworks [37], [38] conduct multi-task learning for occupancy prediction. As the aforementioned approaches all do the occupancy flow tasks as they are trained to be, we discover the variable trend in

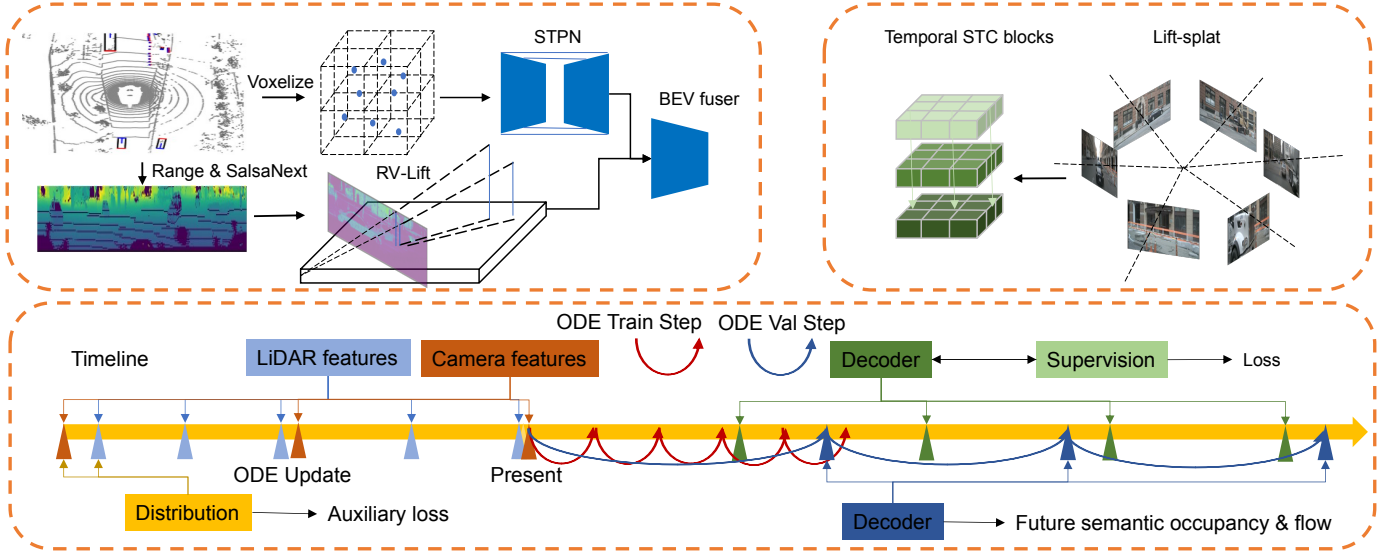


Fig. 1. The framework of FusionMotion. (top left): Spatio-temporal feature extraction for LiDAR point clouds from both BEV and RV views. (top right): Projection from perspective view to BEV via Lift, Splat. (Middle bottom): The SpatialGRU-ODE process operates on the timeline with two stages indicated by the present timestamp, asynchronous multi-sensor deep feature via SpatialGRU-ODE update process and continuous occupancy flow prediction via SpatialGRU-ODE predict process.

occupancy flow and adapt the predictor to a more distant future and finer granularity.

III. PROPOSED APPROACH

A. Framework

The pipeline of FusionMotion is depicted in Fig. 1. Given the autonomous vehicle equipped with LiDARs and ring cameras and sensor data from the previous few seconds, the task is to predict the future semantic occupancy and flow on BEV grids using LiDAR-camera fusion. The framework includes four phases: feature extraction for LiDAR and camera branches, respectively, asynchronous multi-sensor fusion, and continuous occupancy prediction. The upper part is the feature extraction for LiDAR point clouds. We extract LiDAR features using a mixed representation of range view (RV) and bird’s-eye view (BEV). Raw point clouds are densified from multi-frame sweeps and voxelized to binary 3D grids, after which they are passed through a spatio-temporal BEV-based CNN network to produce a BEV representation of non-empty pillars. Another path to raw points is mapping to the range view, using lightweight range-view networks for feature extraction, and projecting to BEV grids with a novel RV-Lift module for unseen or object parts in the rear. The two representations pass through a convolutional BEV fuser. The camera branch consists of a view projector from Lift, Splat [39], and a temporal aggregation block. The SpatialGRU-ODE is the core for the fusion of past BEV latent features from different timestamps and continuous prediction. SpatialGRU-ODE iterates for ODE steps, and updates when a new measurement occurs within a certain ODE cycle and performs future prediction. In the training stage, the loss comes from the supervision of decoded BEV grids as well as an auxiliary probabilistic loss from Kullback-Leibler divergence (KLD) between updated BEV features and latent measurements. In the inference process,

SpatialGRU-ODE predicts via a variable prediction step on-demand only related to the required timestamps for evaluation.

B. Feature Representation

1) *LiDAR Branches*: We adopt both BEV-based and range-based representations for point cloud feature representation. BEV-based representation preprocess voxelized point clouds as binary pillars. The pillar-based feature is extracted via a conventional pillar encoder [14], [40]. Spatio-temporal networks from [21], [22] are an alternative for the extraction of BEV-based features.

RV-Lift. Both pillar and BEV encoders may not be enough for the instance-aware grid-centric prediction, since both representations tend to focus on occupied regions while omitting potential cues for features behind sight-of-view. To this end, we propose RV-Lift, a novel projector that diffuses range features to unseen areas, and serves as a supplement to the pillar and BEV-based encoders.

In comparison to the voxel-based method, RV-based feature representation provides a better understanding of point cloud semantics. Prior arts [41], [42] using range views directly project range view features with points to BEV grids, but this projection cannot foresee possible instance which contains a large portion of invisible voxels. As shown in Fig. 2, RV-Lift treats each range view pixel as a possible ray-caster that extends from the origin to the edge of the perception range. A reasonable assumption is that a measured point corresponds to a location on a non-transparent surface. Each ray before the surface is encoded as free space, and features after the surface are sampled and pooled into BEV grids. The network starts from a lightweight feature extractor on range view, e.g. SalsaNext [43] adopted in this paper. A CNN block lifts each RV pixel feature to a uniform sampling point on each ray. The features along the RV pixel ray before the surface point are

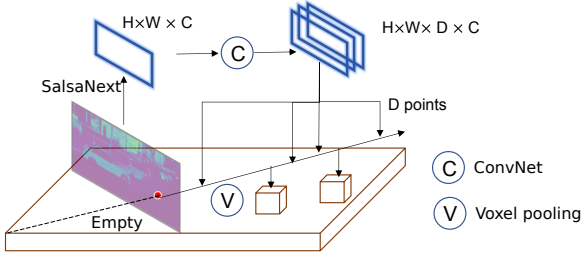


Fig. 2. An Illustration of the RV-Lift module. RV features are lifted to the 3D space along the RV pixel rays and pooled into BEV grids.

set as empty free space. A BEV pooling module aggregates the ray features into BEV grids according to their coordinates.

2) *Camera Branches*: For comparison with prior vision-based BEV prediction methods, we adopt the same Lift, splat(LSS) settings with depth supervision for depth-based view transformation. Note that our framework can trivially adapt to transformer-based view transformation methods such as BEVFormer [28], but their latency is much worse than that of optimized LSS with efficient BEV pooling operators [14], [25].

C. SpatialGRU-ODE

Neural-ODE fundamentals. The Neural-ODE theory is proposed for learning some simple continuous implicit processes in dynamic systems. Given a continuous process h_t , the update process is to calculate the derivatives $\frac{dh(t)}{dt}$ via a neural network,

$$h(t+1) = h_t + f(h_t, \theta_t) \quad (1)$$

$$\frac{dh(t)}{dt} = f(h(t), t, \theta) \quad (2)$$

The core difference between Neural-ODE with other neural networks is that it uses neural networks to parameterize derivatives of hidden states $f(h(t), t, \theta)$ instead of specifying a discrete sequence of hidden layers $h(t)$. Inference of unknown states from derivatives estimation is a natural process with Euler, midpoint, or more complicated solvers provided by the TorchEq toolbox. A simple forward-Euler solver with initial value $h_0 = h(x_0)$ updates the state $y(t)$ iteratively,

$$y(t+1) = y(t) + hf(h(t), t) \quad (3)$$

The Midpoint solver is another alternative to ODE solvers, midpoint solver is calculated like,

$$y(t+1) = y(t) + hf \left[y(t) + \frac{h}{2} f(y(t), t), t + \frac{h}{2} \right] \quad (4)$$

Neural-ODE on GRU blocks. This paper focuses Neural-ODE on modeling continuous time series given sporadic sensor data coming from non-uniform time intervals. The proposed SpatialGRU-ODE is highly inspired by GRU-ODE-Bayes [44], which serves as the foundation component of the proposed spatio-temporal fusion and flow predictor. Gate Recurrent Unit (GRU) is a more concise basic recurrent structure than Long Short Term Memory (LSTM) block, consisting of

reset gate (r_t), update gate (z_t), and update vector (g_t). The update process follows the formula,

$$\begin{aligned} r_t &= \sigma(W_r x_t + U_r h_{t-1} + b_r) \\ z_t &= \sigma(W_z x_t + U_z h_{t-1} + b_z) \\ g_t &= \tanh(W_h x_t + U_h (r_t \odot h_{t-1}) + b_h) \end{aligned} \quad (5)$$

(5) formulates the general process of GRU blocks. With regard to h_t as a BEV feature, SpatialGRU has its state variable h_t with shape $[B, C, H, W]$ where B, C, H, W are the batch size, embedded dims, height, and width. σ is the sigmoid function, and \tanh denotes a CNN block in SpatialGRU settings. x_t is the input state at timestamp t with the same shape as h_t . For simplicity, the update gate $W_r = U_r$, the reset gate $W_z = U_z$, and the GRU init bias $b_r = b_z$. $r_t \odot h_{t-1}$ is the matrix multiplication between reset gate and state. In summary, the update state h_t is calculated as,

$$h_t = z_t \cdot h_{t-1} + (1 - z_t) \cdot g_t = GRU(h_{t-1}, g_t) \quad (6)$$

The amount of change of the state variable is calculated as:

$$\begin{aligned} \Delta h_t &= h_t - h_{t-1} = z_t \cdot h_{t-1} + (1 - z_t) \cdot g_t - h_{t-1} \\ &= (1 - z_t) \cdot (g_t - h_{t-1}) \end{aligned} \quad (7)$$

The derivatives of the state variable are calculated as:

$$\frac{\Delta h(t)}{dt} = (1 - z(t)) \cdot (g(t) - h(t)) \quad (8)$$

GRU-ODE-Bayes has proven the convergence of this process, as is also applicable to the initial state of SpatialGRU-ODE. If $h_0 \in [-1, 1]$, then $h_j(t) \in [-1, 1]$, where j is the index of elements in $h(t)$, as $\left. \frac{dh(t)_j}{dt} \right|_{t:h(t)_j=1} \leq 0$ and

$$\left. \frac{dh(t)_j}{dt} \right|_{t:h(t)_j=-1} \geq 0.$$

Neural-ODE has several nice properties when implemented on GRU models. The learned parametric derivative makes training not constrained by the predetermined task and can be advanced to the untrained state without retraining, which greatly increases flexibility. On the other hand, unlike RNNs, which require emission intervals for updating, the GRU-ODE continuously defined dynamic model can naturally combine data observed at any given time.

In Algorithm 1, the pseudo-code for SpatialGRU-ODE is displayed. The expected output, given state-timestamp pairs from previous multisensor features, is the states of each measured past timestamp and anticipated future timestamp. The ode step may be variable or constant. The Section III-D and Section III-E introduce the two significant functions **ODE_Update** and **ODE_Predict**. During the update procedure, a KL divergence loss is gathered to quantify the similarity between predicted and observed features.

D. Timestamp-agnostic Fusion

Given non-ideal sensor video inputs, timestamp-agnostic fusion attempts to fuse LiDAR and camera BEV features. This strategy will eliminate two crucial limits for multi-sensor fusion. The two assumptions are often guaranteed by dataset creators during preprocessing, but they are not necessarily met in autonomous perception in the real world.

Algorithm 1 The pseudo-code of SpatialGRU-ODE

Input: state-timestamp pairs $[t, m[t]], t \in [t_0, \dots, t_{\text{present}}]$,
 ODE step Δt
Output: $loss_{KLD}$, state-timestamp pairs $[t, h[t]], t \in [t_0, \dots, t_{\text{present}}, \dots, t_{\text{future}}]$.

- 1: Initialize $time = t_0$, $loss_{KLD} = 0$, $h = h_0$
- 2: **for** t_{obs} in $[t_0, \dots, t_{\text{present}}]$ **do**
- 3: **while** $time < t_{\text{obs}}$ **do**
- 4: $h = \text{ODE_Predict}(h, \Delta t)$
- 5: $time += \Delta t$
- 6: **end while**
- 7: $h, loss = \text{ODE_Update}(h, m[t_{\text{obs}}])$
- 8: $loss_{KLD} += loss$
- 9: save $h[t_{\text{obs}}] = h$
- 10: **end for**
- 11: **for** t_{predict} in $[t_{\text{present}+1}, \dots, t_{\text{future}}]$ **do**
- 12: **while** $time < t_{\text{predict}}$ **do**
- 13: $h = \text{ODE_Predict}(h, \Delta t)$
- 14: $time += \Delta t$
- 15: **end while**
- 16: save $h[t_{\text{predict}}] = h$
- 17: **end for**

Cross-sensor synchronization. On most datasets, synchronization is generally ensured by picking temporally nearby measurements as sensor data from the same sample. Synchronization is the essential underlying assumption of multi-sensor spatial alignment and feature fusion.

Uniform data flow. The assumption that sensors operate consistently at all times is stringent. Uniform data flow in spatio-temporal networks will be disrupted by an excessively large burden on the vehicle's computing platform, communication congestion, and occasional sensor failure. Most fusion systems that rely on a single dominating sensor are susceptible to failure if that sensor occasionally malfunctions. Current fusion systems that handle different modalities equally, such as BEVFusion [14], must switch models when switching input between LiDAR/camera/fusion mode, which is inflexible when one sensor experiences periodic errors and immediate recovery.

Fig. 3 presents the network structure for SpatialGRU-ODE update process, which is similar to the bayesian update. sensor measurements are blurred on the source, ordered chronologically, and formulated as multiple timestamp-BEV-feature pairs $[t, h_t]$. The output remains the same shape as the input, but the hidden features are as $\frac{1}{4}$ size of the input for the sake of eliminating memory storage. In order not to degrade the ultimate performance, both state and observation in BEV feature space with shape $[B, C, H, W]$ are implicitly encoded into a smaller feature space $[B, C, H/4, W/4]$ and finally implicit decoded in the same way for occupancy flow decoder. The temporal propagator runs the subsequent ODE step till the arrival of the next observation. When a new observation occurs, the predicted state and new observation are processed into the

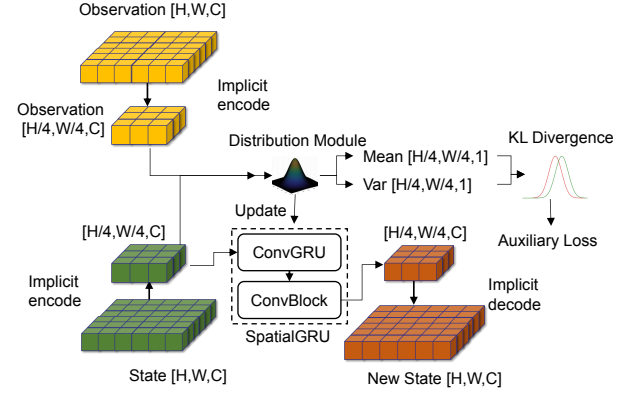


Fig. 3. Illustration of the measurement update process of SpatialGRU-ODE in temporal-agnostic fusion.

distribution module with CNN blocks to obtain the mean and variance of BEV features both with the size $[1, H/4, W/4]$. Means and variances of both features are estimated using KL divergence, an auxiliary loss that reflects the similarity between predicted and measured characteristics. Probabilistic auxiliary loss is calculated as follows:

$$loss_{KLD} = \sum_{j=1}^{H \times W} D_{KL}(p_{\text{state},j} || p_{\text{meas},j}) \quad (9)$$

The core module for the updated BEV feature is a dual-pathway SpatialGRU module, which first propagates the observed and predicted features respectively, then mixes the two hidden states distributions and finally undergoes the weighted summation of two features after the trusting gate and softmax function to generate the final new state.

E. Continuous Occupancy Flow Predictor

Occupancy flow predictor handles multi-frame BEV features from past and present timestamp-agnostic fusion as input and propagates to future steps in an ODE-enabled variational recurrent neural network.

Prior arts with RNNs are hard-coded for emission intervals in future prediction, and at the same time, labels of these time steps are generated for supervision. However, the proposed continuous predictor has the advantage of predicting future occupancy for any given time step even if some time steps are not provided with label supervision. In essence, it models the unit-time changing trend of BEV occupancy flow.

Decoupled from the training granularity, the granularity of temporal prediction horizons is only related to the minimal ODE step in this method. If the lowest granularity (e.g., prediction in 0.05s) is tiny enough for subsequent planning modules, then the discrete process is referred to as continuous in an engineering context. Moreover, it also has the ability to occupancy prediction on request. Additionally, it is capable of occupancy prediction upon request. The required timestamps, which are not confined to the training temporal boundaries, are provided to the model for occupancy flow at these timestamps during the inference process.

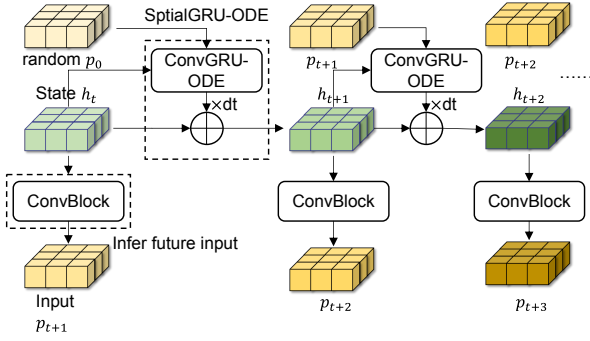


Fig. 4. Illustration of continuous prediction process of SpatialGRU-ODE.

Fig. 4 illustrates the SpatialGRU-ODE procedure. Similar to the update process, the states are implicitly encoded into a smaller feature space. Except for the initial input which is the first BEV feature, the input with shape $[H/4, W/4, C]$ is inherited from the last ODE step. The core module, SpatialGRU-ODE, computes the derivatives of BEV features in unit time intervals via a recurrent block specified in (8). SpatialGRU-ODE may employ either Euler or Midpoint solver for the update and fixed or variable ODE time step. To obtain the projected states, the derivatives are multiplied by delta time dt and added to the initial states. A CNN block is used to infer the next input from the current state in order to make the subsequent prediction. Only states near to the needed timestamps with supervision (closer than half of the minimum ode step) are preserved and decoded in the BEV decoder for supervision. Thus, the prediction time step dt is not always constant and uniform, and supervision signals are not required for each future timestamp.

F. Decoders, Loss and Post-processing

The decoders are inherited from FIERY [26], [36], [37]. Five distinct decoders produce centerness regression, BEV segmentation, offset to the centers, future flow vectors, and instance given the BEV feature representation of past and future frames. The shared BEV feature will be input into a shared Resnet18 BEV backbone and five independent CNN blocks.

The loss design consists of spatial regression loss, segmentation loss, and probabilistic loss. Spatial regression loss is responsible for regressing centerness and offsets in a L1 loss or mean square error(MSE/L2) loss manner. Segmentation loss is the computation of the cross-entropy loss on multi-frame BEV semantic grids from the past to the future. Probabilistic loss computes the divergence between updated BEV features and measurement features with regard to their mean and variance on BEV grids. The overall loss is calculated as follows:

$$Loss = \lambda_1 * L_{seg} + \lambda_2 * L_{spatial} + \lambda_3 * L_{kld} \quad (10)$$

In (10), λ is the weight of each loss. For simplicity, we set $\lambda_1 = 0.5$, $\lambda_2 = 0.5$, and $\lambda_3 = 1.0$.

The post-processing unit generates a unified instance segmentation and its motion flow by computing the offset from each center point and surrounding points to the center point.

Then it recognizes distinct instances and formulates motion flow data.

IV. EXPERIMENTS

A. Experiment Setup

1) **Datasets:** **nuScenes.** nuScenes [45] dataset is a public large-scale autonomous driving dataset collected by Motional. NuScenes dataset provides a full sensor suite including 1 top LiDAR, 6 cameras, 5 radars, GPS, and IMU, all with 360° coverage of the surroundings. It contains 1000 scenes, each lasting 20 seconds, of which annotations of 850 scenes at 2Hz are available. We utilize LiDAR point clouds and multi-view images, which are captured at 20Hz and 10Hz respectively. The training and validation splits are the same as previous arts [21], [26], [36]–[38], with 28130 samples for training and 6019 samples for validation.

Lyft L5. Lyft dataset [46] is another large-scale autonomous dataset provided by Lyft. This dataset contains 180 scenes, each lasting 25-45s in length and annotated at 5Hz. The data is collected with 7 cameras and 3 LiDARs. This paper uses 6 ring cameras and the top LiDAR from its sensor suite, which has a 360° field of view. We use splits from FIERY [26], which include 16000 training samples and 4000 validation samples.

2) **Metrics:** The occupancy flow prediction is formulated as a video panoptic prediction task [47]. We use Intersection over Union (IoU) to measure the semantic segmentation quality of each frame, and video panoptic quality (PQ), recognition quality (RQ), and segmentation quality (SQ) to measure both the accuracy of instance segmentation and consistency of instance detection. VPQ is computed as:

$$\begin{aligned} VPQ &= \sum_{t=0}^H \frac{\sum_{(p_t, q_t) \in TP_t} \text{IoU}(p_t \cdot q_t)}{|TP_t| + \frac{1}{2}|FP_t| + \frac{1}{2}|FN_t|} \\ &= \sum_{t=0}^H \frac{|TP_t|}{|TP_t| + \frac{1}{2}|FP_t| + \frac{1}{2}|FN_t|} = SQ \cdot RQ \end{aligned} \quad (11)$$

3) **Implementation Details:** **Task details.** Without further marks, the standard occupancy prediction task is to take the past 1.0s sensor data for input, which is 3 key frames in nuScenes (5 key frames in Lyft), predict the motion in the future 4 key frames (10 key frames in Lyft) and compute the aforementioned metrics around the ego vehicle for 2.0s.

Data details. For a fair comparison with prior works, we follow most of the basic configurations for pre-processing images and point clouds from both prior LiDAR-based and vision-based methods.

The BEV occupancy labels are generated from 3D box labels. 3D bounding boxes of the vehicles are projected to BEV to form the BEV occupancy grid and instance map. For all experiments, the perception range is set as $[100m, 100m]$ and the grid resolution is set as $0.25m$.

The algorithm input six images for only key frames at 2Hz and LiDAR points from the aggregation of past sweeps. At key frames, the images are resized to 224×480 pixels for each frame. The point cloud is collected from the top LiDAR. A common approach for denser point clouds is to aggregate

point clouds of non-key frames to the current frame. After that, point clouds are voxelized at 5Hz using a grid resolution of $200 \times 200 \times 13$ voxels. For the range view branch, point clouds are projected to the range picture with 2048×64 pixels. Empty pixels are marked as -1 .

Model details. The framework is implemented on Pytorch 1.10.2 and Pytorch Lightning 1.2.5. Pretrained models are not used except for image encoders. The image encoder is EfficientNet-b0 [48] pretrained by Torchvision. The optimizer is AdamW with a learning rate $1e-4$. The learning strategy is cosine annealing with a weight decay 0.01. The training schedule is set as 20 epochs. All training schedules are implemented by 8xA6000 GPUs.

4) *Run-time Analysis:* Table. I compares the run-time training memory of the proposed method with baselines in different dataset settings. As the time interval becomes denser, the training cost for standard GRU units becomes unaffordable, whereas the proposed method is more adaptable. For standard 4-keyframe supervision, FusionMotion only requires +2G more memory compared to a BEVFusion-style implementation. As the density of supervision signals increases, the ODE approach requires $-4G$ less memory than standard GRU counterparts.

The inference speed of FusionMotion is measured by the average time required to process validation samples over 250 forward passes on a laptop equipped with a single RTX3090. As FusionMotion inherits the same framework and modules from FIERY [26], it is compared with FIERY [26] and StretchBEV [36]. For the settings of the standard task and variable ode steps, FusionMotion runs at 0.7032s/sample, slightly slower than FIERY(0.6436s/sample) and StretchBEV(0.6469s/sample) reported in [36], as FusionMotion adds the LiDAR branch. The SpatialGRU-ODE works at a similar speed with prior temporal modules. The inference speed for tasks with finer granularity (40-frame experiment) is 1.1075s per sample. Obviously, higher prediction frequencies harm the run-time delay. Therefore, sparse prediction based on variable ODE step by request is recommended more.

TABLE I
RUNTIME ANALYSIS OF TRAINING COST OF DIFFERENT MODEL CONFIGS.
'OOM' DENOTES OUT-OF-MEMORY FOR ONE BATCH IN A SINGLE A6000 GPU (48G MEMORY)

Dataset	Config	Supervised frames	Memory
nuScenes	GRU-base	4	11G
nuScenes	GRU-ODE	4	13G
nuScenes	GRU-base	40	39G
nuScenes	GRU-ODE	40	OOM
Lyft	GRU-base	10	28G
Lyft	GRU-ODE	10	24G

B. Main Results

In this section, we seek to answer three questions about the performance of FusionMotion. (1) Does the model work better than published state-of-the-art algorithms designed for the same task? (2) Does the model achieve comparable fusion performance compared to state-of-the-art fusion strategies,

specifically BEVFusion [14]? (3) Is the model able to generalize to untrained temporal horizons and intervals only using checkpoints trained for the standard task?

1) *Comparison with the State-of-the-art Algorithms:* We compare the performance of the proposed method to that of previously published methods. All methods are prepared for a standard instance flow segmentation and prediction task introduced in FIERY [26]. FusionMotion uses the same image and point cloud pre-processing pipelines as most vision- and LiDAR-based methods. Fig. 5 illustrates some examples covering diverse scenarios, including sequences collected from urban and highway. The weather conditions are selected from sunny, overcast, rainy, and night.

Baselines.

Vision track. FIERY [26] is the first practice for end-to-end stochastic occupancy flow prediction. StretchBEV [36]¹ uses a variational autoencoder for learning implicit temporal dynamics and future prediction in a decoupled style. ST-P3 [37] is the first end-to-end planning framework that considers occupancy prediction. BEVerse [38] is the first multi-task model for both object- and grid-level perception.

LiDAR track. MotionNet [22] is the first practice for learning BEV grid motion using a simple spatial-temporal voxel-based backbone (STPN). BE-STI [21] develops the backbone with two new blocks, SeTE and TeSe to enhance temporal feature representation. Since LiDAR track algorithms are not originally proposed for this task, we reimplement them using original BEV backbones and prediction heads for this task.

Results. Comparisons of methods implemented in the nuScenes dataset are shown in Table. II. Compared to the state-of-the-art end-to-end occupancy networks, the proposed FusionMotion achieves the best of all metrics while significantly outperforming other single-modality methods. As the first algorithm of LiDAR-camera fusion in occupancy prediction fields, FusionMotion surpasses the best vision-based BEVerse [38] with a larger backbone SwinTransformer-small [49] by +7.0 in terms of IoU and 10.0 in terms of VPQ, and the best LiDAR-based BE-STI [21] +7.7 points in terms of IoU and 5.1 points in terms of VPQ.

Comparisons of methods implemented in the Lyft L5 dataset are shown in Table. III. FusionMotion achieves the best of all metrics while surpassing baseline methods by a large margin, which surpasses ST-P3 [37] by +20.6 points in terms of semantic IoU and +23.5 points in terms of VPQ.

As a similar task to flow prediction, we also compare the performance of BEV segmentation of intermediate representations with prior arts in Table. IV. We evaluate two main traffic agent categories, vehicle, and pedestrian by IoU metric. With timestamp-agnostic camera-LiDAR fusion by SpatialGRU-ODE, FusionMotion also achieves impressive progress in typical agent segmentation. It surpasses ST-P3 [37] by +10.7 for vehicles and +22.7 for pedestrians.

2) *Comparison with State-of-the-art Fusion Strategies:* We compare the proposed SpatialGRU-ODE with state-of-

¹StretchBEV-P uses ground-truth labels of past frames as a posterior for prediction, which is unfair for comparison with end-to-end occupancy prediction, so only StretchBEV without labels is compared in the table.

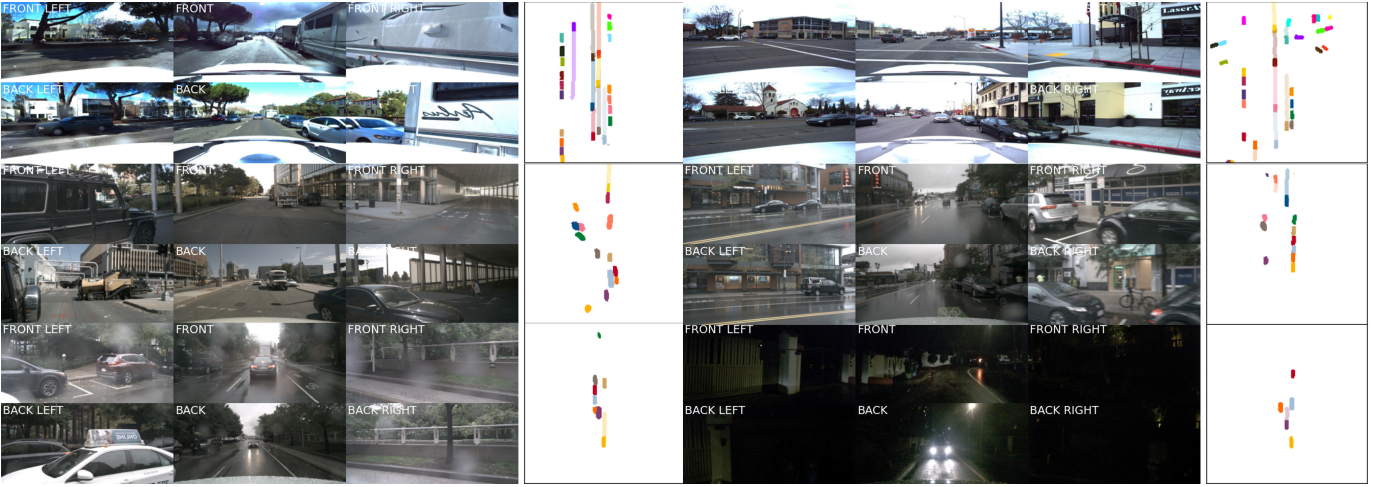


Fig. 5. Visualization of FusionMotion for diverse driving scenarios. Different colors represent different instances of the agents, and light colors represent the future occupancy of the agents. (top): samples from Lyft dataset, highway (left), and urban (right). (middle and bottom): samples from nuScenes dataset, sunny (middle left), overcast after rain (middle right), rainy (bottom left), and night (bottom right). The proposed method works well in all challenging driving scenarios.

TABLE II

COMPARISON WITH THE STATE-OF-THE-ART METHODS FOR INSTANCE-AWARE OCCUPANCY FLOW PREDICTION ON THE nuSCENES [45] VALIDATION SET. 'C' DENOTES VISION-ONLY METHODS, 'L' DENOTES LiDAR-BASED METHODS, AND 'LC' DENOTES A LiDAR-CAMERA FUSION METHOD.

Method	Modality	Backbone	Future Semantic Seg. IoU \uparrow	Future Instance Seg. PQ \uparrow	SQ \uparrow	RQ \uparrow
Static*	C	Effi-B4	32.2	27.6	70.1	39.1
FIERY* [26]	C	Effi-B4	37.0	30.2	70.2	42.9
StretchBEV [36]	C	Effi-B4	37.1	29.0	-	-
BEVerse [38]	C	Swin-tiny	38.7	33.3	70.6	47.2
BEVerse [38]	C	Swin-small	40.8	36.1	70.7	51.1
ST-P3 Gaus. [37]	C	Effi-B4	38.6	31.7	70.2	45.2
ST-P3 Ber. [37]	C	Effi-B4	38.9	32.1	70.4	45.6
MotionNet [21]	L	STPN	37.2	38.9	75.6	51.4
BE-STI	L	BESTI-STPN	40.1	41.0	75.5	54.3
FusionMotion	LC	Effi-B4 + STPN + RV-Lift	47.8	46.1	75.8	60.8

TABLE III

COMPARISON WITH THE STATE-OF-THE-ART METHODS FOR FUTURE INSTANCE SEGMENTATION (2.0s) ON LYFT L5 AV [46] VALIDATION SET.
*: RESULTS REPORTED IN [26].

Method	IoU \uparrow	PQ \uparrow	SQ \uparrow	RQ \uparrow
Static*	24.1	20.7	-	-
Extrapolation model*	24.8	21.2	-	-
FIERY* [26]	36.3	27.2	-	-
ST-P3 [37]	36.3	32.4	71.1	45.5
FusionMotion	56.9	55.9	78.1	71.9

TABLE IV

COMPARISON WITH THE STATE-OF-THE-ART METHODS FOR BEV SEGMENTATION OF VEHICLES AND PEDESTRIANS ON nuSCENES [45] VALIDATION SET.

Method	Vehicle / IoU	Pedestrian / IoU
VED [50]	23.3	11.9
VPN [51]	28.2	10.3
PON [52]	27.9	13.9
Lift-Splat [39]	31.2	15.0
IVMP [53]	34.0	17.4
FIERY [26]	38.0	17.2
ST-P3 [37]	40.1	14.5
FusionMotion	50.8	37.2

the-art fusion strategies. SpatialGRU-ODE features temporal without spatial fusion, with no requirement of sensor data synchronization and time uniformity. In order to validate the performance of SpatialGRU-ODE, baselines with certain common assumptions are prepared.

Baselines. Synchronous fusion. The process is first multi-modal spatial fusion, then mixed-modal temporal fusion, and finally standard GRU modules. The assumption is that, at each frame, LiDAR points are tightly synchronized and fused with the nearest images. Spatial fusion follows the same

methodology as BEVFusion [14]. This process requires strict synchronization and weak time interval uniformity.

Asynchronous fusion: The process is first single-modal temporal fusion, then standard GRU modules, and finally mixed-modal spatial fusion on future timestamps. Single-modal temporal fusion is first performed using the spatio-temporal convolution (STC) unit, and then spatial fusion is performed during prediction. The assumption is that the

perception and prediction times are strictly uniform. This process requires only weak synchronization and strict time interval uniformity.

Results. As shown in Table. V, asynchronous fusion is inferior to synchronous fusion and SpatialGRU-ODE for both datasets. For nuScenes dataset, the ordinary temporally-synchronized fusion approach performs the best. SpatialGRU-ODE performs -2.4 points in terms of IoU and -0.9 in terms of VPQ, slightly less than BEVFusion [14]. For Lyft dataset, SpatialGRU-ODE outperforms synchronized fusion. It performs $+2.3$ points in terms of IoU and $+0.2$ in terms of VPQ more than BEVFusion [14].

The difference from comparison with BEVFusion on different datasets is possibly related to the sparsity of supervision. On nuScenes dataset, the predictor is supervised approximately every $0.5s$, while the internal ode step is $0.05s$, which means the predictors need to update 10 rounds before strong supervision. On Lyft dataset, the predictor is supervised every $0.2s$, which only needs 4 rounds for possible supervision. Though fully-dense supervision at each time step is unaffordable, sparser supervision may impair the final prediction performance.

TABLE V
COMPARISON WITH THE BASELINE FUSION METHODS FOR FUTURE INSTANCE SEGMENTATION (2.0s) ON nuSCENES VALIDATION SET. FUSIONMOTION-ODE IS COMPARED WITH DIFFERENT FUSION MODES. SPATIAL FUSION IS CONDUCTED IN THE SAME WAY AS BEVFUSION. 'SPATIAL THEN TEMPORAL' IS FOR SYNCHRONOUS MODE, AND 'TEMPORAL THEN SPATIAL' IS FOR ASYNCHRONOUS MODE.

Fusion mode	IoU↑	PQ↑	SQ↑	RQ↑
nuScenes dataset				
Spatial then temporal	50.2	47.0	75.6	63.0
Temporal then spatial	44.7	42.7	74.6	57.2
SpatialGRU-ODE	47.8	46.1	75.8	60.8
Lyft L5 AV dataset				
Spatial then temporal	54.6	55.7	78.0	71.4
Temporal then spatial	50.4	50.2	75.2	66.7
SpatialGRU-ODE	56.9	55.9	78.1	71.9

3) Demonstration of Continuous Occupancy Prediction:

We demonstrate two abilities of the proposed method for continuous occupancy prediction: prediction in different temporal horizons and different time intervals. The training process for both evaluations is the same as the standard task but the inference process outputs information on demand.

Prediction in different temporal horizons. Extending FusionMotion to different prediction domains does not need re-training of the model. The previous prediction algorithm needs to be trained according to the present prediction time domain, and it is necessary to prepare farther truth values. In our work, only the model trained for the standard prediction task is used for inference when the supervised signals only cover from 1.0s to 3.0s information.

Table. VI shows the prediction result of FusionMotion which extends the temporal horizons from 1.0s to 9.0s. Baselines reported in [36] are trained for different lengths of temporal horizons. FusionMotion-ODE shows excellent performance in variable prediction length without retraining.

TABLE VI
COMPARISON OF OCCUPANCY FLOW PREDICTION FOR ANY TEMPORAL HORIZONS.

Method	Pred	IoU↑	PQ↑	SQ↑	RQ↑
FIERY	2s	35.8	29.0	-	-
	4s	30.1	23.6	-	-
	6s	26.7	20.9	-	-
StretchBEV	2s	37.1	29.0	-	-
	4s	32.5	23.8	-	-
	6s	28.4	21.0	-	-
FusionMotion with SpatialGRU-ODE	2s	48.0	40.8	71.5	57.1
	3s	43.4	35.5	71.1	50.1
	4s	38.7	31.4	70.7	44.4
	6s	31.7	24.6	70.0	35.1
	8s	23.1	18.6	69.7	26.8

Similar to prior arts which extend prediction horizons to farther future, FusionMotion shows a gradual performance decay, approximately -4 in terms of IoU and -5 in terms of VPQ per lengthened second for prediction, as occupancy predictors are less capable of processing long-term dynamics than trajectory predictors. However, FusionMotion propagates temporal dynamics stably for unforeseen temporal horizons.

Prediction in different time intervals. This section demonstrates the ability of FusionMotion for accurate prediction at any given timestamps in the prediction horizons. Validation of continuous occupancy prediction is designed to obtain high-frequency occupancy prediction results and visually illustrate the output of 20Hz, totaling 40 frames. As both nuScenes and Lyft L5 datasets do not provide object labels on non-keyframes, dense continuous instance occupancy prediction are qualitatively demonstrated in Fig. 6. A video demo for continuous occupancy prediction for more scenarios is available in the GitHub repository².

In the 40-frame prediction visualization, the static instances remain static overall with only minor changes in the perception range. Though grid-centric perception is discrete in essence, the prediction results show that FusionMotion successfully learns the temporal dynamics in continuous time series.

C. Ablation Study

1) Ablation of LiDAR feature representation methods:

This section presents different LiDAR feature representation methods, their combinations, and LiDAR-camera fusions. The experiments start with a commonly used pillar encoder, but the performance of the pillar encoder is weak by 8.1 and 10.8 in terms of IoU and VPQ. A possible reason is that as there is no box constraint and corresponding detection heads (e.g. anchor head or center head) in occupancy flow settings, it is difficult for the pillar encoder to illuminate an instance with a large portion of unobserved empty pillars. Moreover, the STPN series method works well alone, as the networks mainly consist of 2D convolutional blocks on BEV grids. Among them, BE-STI has $+2.9$ and $+3.0$ points gain in terms of IoU and VPQ compared to STPN. However, the performance of BE-STI decreases when fusing with range or camera BEV features.

²<https://github.com/synsin0/FusionMotion>

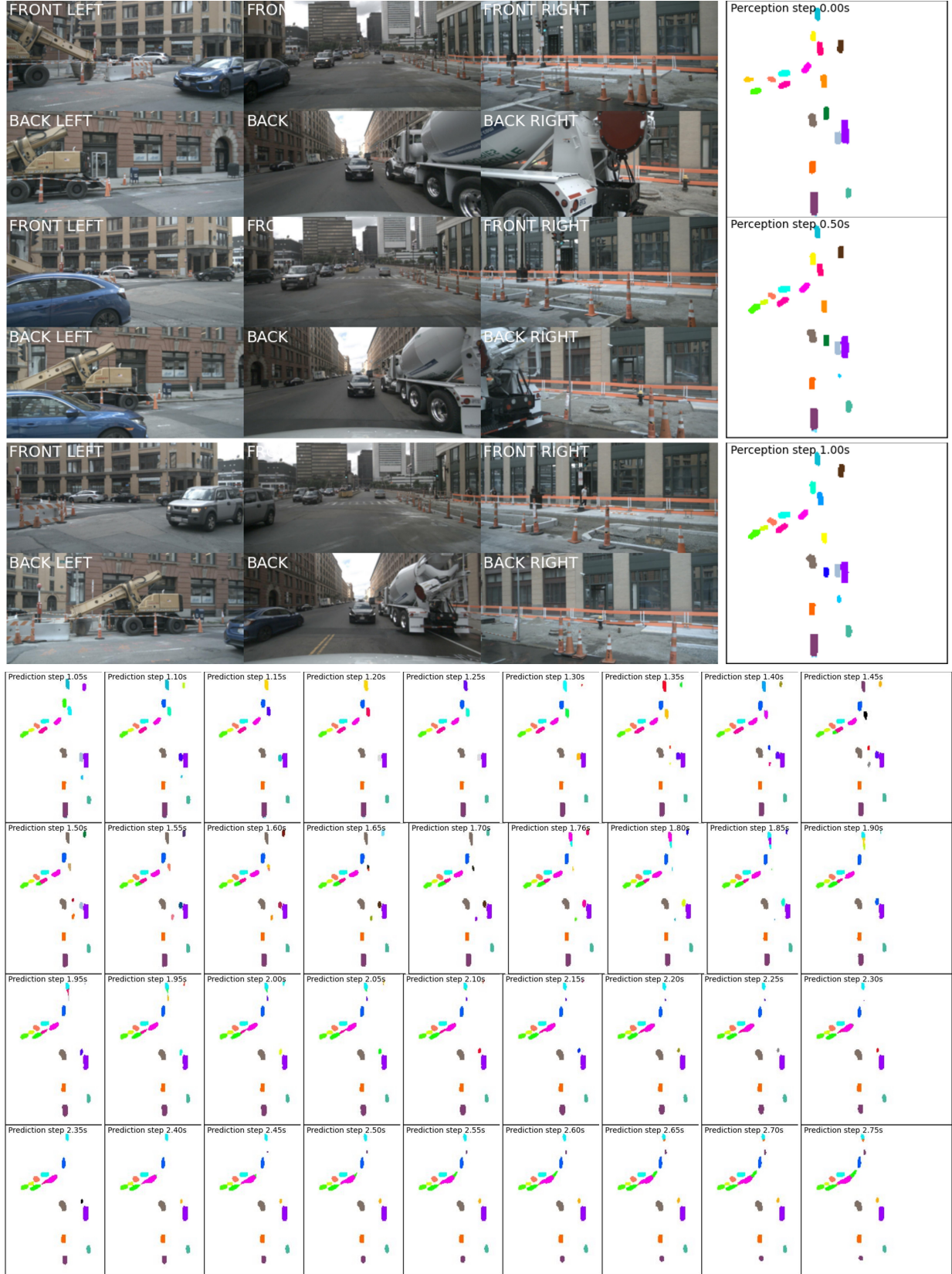


Fig. 6. Visualization of FusionMotion for continuous panoptic occupancy flow prediction at a busy intersection. Given 3 key-frame cameras inputs and asynchronous 5 key-frame LiDAR inputs, we are able to accurately predict the continuous trend of dynamic trend(front left view) only with sparse supervision.

Fusion of STPN and RV-Lift has slightly better performance than BE-STI by +0.4 and +0.9 points in terms of IoU and VPQ.

Not surprisingly, LiDAR-camera fusion outperforms LiDAR-based methods, as images compensate for the semantic loss of LiDAR-based methods. RV-Lift is shown as a useful complement for modeling backward features, with a +1.5 and +1.2 points in terms of IoU and VPQ. The final model with all feature representation techniques achieves the best performance with 50.2 and 47.0 in terms of IoU and VPQ.

TABLE VII
COMPARISON OF FEATURE REPRESENTATION STRUCTURE IN LiDAR BRANCH AND L-C FUSION METHODS ON nuScenes VALIDATION SET

LiDAR branch	IoU↑	PQ↑	SQ↑	RQ↑
LiDAR only				
PillarEncoder	8.1	10.8	27.0	40.0
STPN	37.2	38.9	75.6	51.4
RV-Lift	31.4	18.3	72.8	18.5
BESTI-STPN	40.1	41.0	75.5	54.3
STPN + RV-Lift	40.5	41.9	75.6	55.4
LiDAR-camera fusion				
Effi-B4 + RV-Lift	43.0	36.3	71.2	51.5
Effi-B4 + STPN	48.7	45.8	74.6	61.3
Effi-B4 + STPN + RV-Lift	50.2	47.0	75.6	63.0

2) *Ablation of ODE solvers*: ODE solvers are vital low-level tools for a Neural-ODE-based framework. As the state variable in FusionMotion is rather high-dimensional, two basic ode solvers, Euler and midpoint solver are compared in Table. VIII on two datasets.

TABLE VIII
COMPARISON WITH PREDICTION USING DIFFERENT ODE SOLVERS.

ODE Solver	IoU↑	PQ↑	SQ↑	RQ↑
nuScenes dataset				
Euler	47.8	42.9	73.5	58.6
Midpoint	47.8	45.1	74.5	60.8
Lyft L5 AV dataset				
Euler	56.9	55.9	78.1	71.9
Midpoint	55.0	56.7	78.2	72.4

In both cases, the midpoint solver yields superior instance panoptic quality, surpassing the Euler solver by 2.2 points on nuScenes dataset and 0.8 points on Lyft dataset. On nuScenes dataset, the midpoint solver shows similar IoU with the Euler solver, but on Lyft dataset, the midpoint solver performs worse semantic segmentation by -1.9 .

3) *Ablation of ODE Update Intervals*: ODE update interval determines the minimum granularity of occupancy prediction. As shown in the run-time analysis, more prediction frames lead to higher latency. This section ablates the relationship between final performance and different update intervals. For a standard task, the ode step is set to 0.05, 0.1, and 0.5 for comparison. An alternative is to propagate to the nearest measurement timestamp, dubbed the variable ode step in this paper.

TABLE IX
COMPARISON OF PREDICTION UNDER DIFFERENT ODE STEPS.

Step	IoU↑	PQ↑	SQ↑	RQ↑
nuScenes dataset				
0.05	47.8	46.1	75.8	60.8
0.1	47.7	43.0	73.7	58.4
0.5	47.3	42.1	73.3	57.4
Variable	48.2	43.9	73.9	58.8
Lyft L5 dataset				
0.05	56.9	55.9	78.1	71.9
Variable	54.0	53.5	77.4	69.7

For the standard task, the given time interval between two adjacent supervision or inference timestamps usually varies in $[0.4, 0.6]$. In general, the finer a single update is divided during the ODE update process, the higher the final prediction accuracy. It is also intuitive that a higher update frequency may eliminate continuous errors. As shown in Table. IX, the predictor with interval $0.05s$ surpasses interval $0.1s$ by 0.1 and 3.1 in terms of IoU and VPQ, and interval $0.5s$ by 0.5 and 3.1 in terms of IoU and VPQ. Remarkably, the variable time step update also shows nice performance, which is +0.5 and -2.2 in terms of IoU and VPQ when compared to the predictor with ODE step $0.05s$. A variable time step updater strikes a good balance between precision and inference speed.

D. Discussion

Flexibility is the core advantage of the proposed FusionMotion. The SpatialGRU-ODE decouples the supervision in the training process and outputs in the inference process, by modeling the derivatives of BEV grids and propagating future grid states to required timestamps. As for the training process, the supervised signal of future frames can be dense or sparse, but the extremely sparse supervised signal in the prediction step may degrade the performance of SpatialGRU-ODE, as the state may be updated too many times until the next supervised frame. In contrast, the denser supervised signal can strengthen the method to surpass the state-of-the-art synchronized spatial fusion method. For accurate inference at future timestamps with low latency, SpatialGRU-ODE with variable time step, which is closely related to different prediction requests, is the best practice.

V. CONCLUSION

We present FusionMotion as the first practice for end-to-end multi-sensor fusion-based occupancy flow prediction. The motivation is to loosen the uniform sampling and synchronization restrictions in multi-sensor deep fusion and generalize the occupancy flow prediction to the untrained task domain. We introduce one variant of Neural-ODE, GRU-ODE, in network design of flow prediction, which primarily innovates the modeling of the continuous trend of implicit spatial BEV features in sporadically observed, continuously predicted time series, and realizes the function of continuous occupancy prediction on any temporal horizons and time intervals all with a single checkpoint without re-training. We hope that this work

will inspire more Neural-ODE applications and insights into the design of the temporal module for automotive perception.

ACKNOWLEDGMENTS

This work was supported in part by the National Natural Science Foundation of China under Grants U22A20104, and Beijing Municipal Science and Technology Commission (Grant No.Z221100008122011). This work was also sponsored by Tsinghua University-DiDi Joint Research Center for Future Mobility.

REFERENCES

- [1] G. Tanzmeister and D. Wollherr, "Evidential grid-based tracking and mapping," *IEEE Transactions on Intelligent Transportation Systems*, vol. 18, no. 6, pp. 1454–1467, 2016.
- [2] D. Nuss, S. Reuter, M. Thom, T. Yuan, G. Krehl, M. Maile, A. Gern, and K. Dietmayer, "A random finite set approach for dynamic occupancy grid maps with real-time application," *International Journal of Robotics Research*, vol. 37, no. 8, pp. 841–866, 2018.
- [3] D. Feng, C. Haase-Schütz, L. Rosenbaum, H. Hertlein, C. Gläser, F. Timm, W. Wiesbeck, and K. Dietmayer, "Deep multi-modal object detection and semantic segmentation for autonomous driving: Datasets, methods, and challenges," *IEEE Transactions on Intelligent Transportation Systems*, vol. 22, no. 3, pp. 1341–1360, 2021.
- [4] K. Huang, B. Shi, X. Li, X. Li, S. Huang, and Y. Li, "Multi-modal sensor fusion for auto driving perception: A survey," *arXiv preprint arXiv:2202.02703*, 2022.
- [5] S. Vora, A. H. Lang, B. Helou, and O. Beijbom, "Pointpainting: Sequential fusion for 3d object detection," in *Proceedings of the IEEE/CVF conference on computer vision and pattern recognition*, 2020, pp. 4604–4612.
- [6] C. Wang, C. Ma, M. Zhu, and X. Yang, "Pointaugmenting: Cross-modal augmentation for 3d object detection," in *Proceedings of the IEEE/CVF Conference on Computer Vision and Pattern Recognition*, 2021, pp. 11 794–11 803.
- [7] S. Pang, D. Morris, and H. Radha, "Clocs: Camera-lidar object candidates fusion for 3d object detection," in *2020 IEEE/RSJ International Conference on Intelligent Robots and Systems (IROS)*. IEEE, 2020, pp. 10 386–10 393.
- [8] J. Ku, M. Mozifian, J. Lee, A. Harakeh, and S. L. Waslander, "Joint 3d proposal generation and object detection from view aggregation," in *2018 IEEE/RSJ International Conference on Intelligent Robots and Systems (IROS)*. IEEE, 2018, pp. 1–8.
- [9] C. R. Qi, W. Liu, C. Wu, H. Su, and L. J. Guibas, "Frustum pointnets for 3d object detection from rgb-d data," in *Proceedings of the IEEE conference on computer vision and pattern recognition*, 2018, pp. 918–927.
- [10] Z. Wang and K. Jia, "Frustum convnet: Sliding frustums to aggregate local point-wise features for amodal 3d object detection," in *2019 IEEE/RSJ International Conference on Intelligent Robots and Systems (IROS)*. IEEE, 2019, pp. 1742–1749.
- [11] R. Nabati and H. Qi, "Centerfusion: Center-based radar and camera fusion for 3d object detection," in *Proceedings of the IEEE/CVF Winter Conference on Applications of Computer Vision*, 2021, pp. 1527–1536.
- [12] X. Chen, H. Ma, J. Wan, B. Li, and T. Xia, "Multi-view 3d object detection network for autonomous driving," in *Proceedings of the IEEE conference on Computer Vision and Pattern Recognition*, 2017, pp. 1907–1915.
- [13] X. Chen, T. Zhang, Y. Wang, Y. Wang, and H. Zhao, "Futr3d: A unified sensor fusion framework for 3d detection," *arXiv preprint arXiv:2203.10642*, 2022.
- [14] Z. Liu, H. Tang, A. Amini, X. Yang, H. Mao, D. Rus, and S. Han, "Bevfusion: Multi-task multi-sensor fusion with unified bird's-eye view representation," *arXiv preprint arXiv:2205.13542*, 2022.
- [15] N. Hendy, C. Sloan, F. Tian, P. Duan, N. Charchut, Y. Xie, C. Wang, and J. Philbin, "Fishing net: Future inference of semantic heatmaps in grids," *arXiv preprint arXiv:2006.09917*, 2020.
- [16] A. W. Harley, Z. Fang, J. Li, R. Ambrus, and K. Fragkiadaki, "A simple baseline for bev perception without lidar," *arXiv preprint arXiv:2206.07959*, 2022.
- [17] X. Bai, Z. Hu, X. Zhu, Q. Huang, Y. Chen, H. Fu, and C.-L. Tai, "Transfusion: Robust lidar-camera fusion for 3d object detection with transformers," in *Proceedings of the IEEE/CVF Conference on Computer Vision and Pattern Recognition*, 2022, pp. 1090–1099.
- [18] Y. Li, Y. Chen, X. Qi, Z. Li, J. Sun, and J. Jia, "Unifying voxel-based representation with transformer for 3d object detection," *arXiv preprint arXiv:2206.00630*, 2022.
- [19] Z. Chen, Z. Li, S. Zhang, L. Fang, Q. Jiang, F. Zhao, B. Zhou, and H. Zhao, "Autoalign: Pixel-instance feature aggregation for multi-modal 3d object detection," *arXiv preprint arXiv:2201.06493*, 2022.
- [20] Z. Chen, Z. Li, S. Zhang, L. Fang, Q. Jiang, and F. Zhao, "Autoalignv2: Deformable feature aggregation for dynamic multi-modal 3d object detection," *arXiv preprint arXiv:2207.10316*, 2022.
- [21] Y. Wang, H. Pan, J. Zhu, Y.-H. Wu, X. Zhan, K. Jiang, and D. Yang, "Besti: Spatial-temporal integrated network for class-agnostic motion prediction with bidirectional enhancement," in *Proceedings of the IEEE/CVF Conference on Computer Vision and Pattern Recognition*, 2022, pp. 17 093–17 102.
- [22] P. Wu, S. Chen, and D. N. Metaxas, "MotionNet: Joint Perception and Motion Prediction for Autonomous Driving Based on Bird's Eye View Maps," *Proceedings of the IEEE Computer Society Conference on Computer Vision and Pattern Recognition*, pp. 11 382–11 392, 2020.
- [23] X. Chen, S. Shi, B. Zhu, K. C. Cheung, H. Xu, and H. Li, "Mppnet: Multi-frame feature intertwining with proxy points for 3d temporal object detection," *arXiv preprint arXiv:2205.05979*, 2022.
- [24] J. Huang and G. Huang, "Bevdet4d: Exploit temporal cues in multi-camera 3d object detection," *arXiv preprint arXiv:2203.17054*, 2022.
- [25] Y. Li, Z. Ge, G. Yu, J. Yang, Z. Wang, Y. Shi, J. Sun, and Z. Li, "Bevdepth: Acquisition of reliable depth for multi-view 3d object detection," *arXiv preprint arXiv:2206.10092*, 2022.
- [26] A. Hu, Z. Murez, N. Mohan, S. Dudas, J. Hawke, V. Badrinarayanan, R. Cipolla, and A. Kendall, "FIERY: Future Instance Prediction in Bird's-Eye View from Surround Monocular Cameras," *Proceedings of the IEEE International Conference on Computer Vision*, pp. 15 253–15 262, 2021.
- [27] J. Park, C. Xu, S. Yang, K. Keutzer, K. Kitani, M. Tomizuka, and W. Zhan, "Time will tell: New outlooks and a baseline for temporal multi-view 3d object detection," *arXiv preprint arXiv:2210.02443*, 2022.
- [28] Z. Li, W. Wang, H. Li, E. Xie, C. Sima, T. Lu, Q. Yu, and J. Dai, "Bevformer: Learning bird's-eye-view representation from multi-camera images via spatiotemporal transformers," *arXiv preprint arXiv:2203.17270*, 2022.
- [29] Y. Jiang, L. Zhang, Z. Miao, X. Zhu, J. Gao, W. Hu, and Y.-G. Jiang, "Polarformer: Multi-camera 3d object detection with polar transformers," *arXiv preprint arXiv:2206.15398*, 2022.
- [30] Y. Liu, J. Yan, F. Jia, S. Li, Q. Gao, T. Wang, X. Zhang, and J. Sun, "PetrV2: A unified framework for 3d perception from multi-camera images," *arXiv preprint arXiv:2206.01256*, 2022.
- [31] Z. Qin, J. Chen, C. Chen, X. Chen, and X. Li, "Uniformer: Unified multi-view fusion transformer for spatial-temporal representation in bird's-eye-view," *arXiv preprint arXiv:2207.08536*, 2022.
- [32] R. Mahjourian, J. Kim, Y. Chai, M. Tan, B. Sapp, and D. Anguelov, "Occupancy flow fields for motion forecasting in autonomous driving," *IEEE Robotics and Automation Letters*, vol. 7, no. 2, pp. 5639–5646, 2022.
- [33] W. Luo, B. Yang, and R. Urtasun, "Fast and furious: Real time end-to-end 3d detection, tracking and motion forecasting with a single convolutional net," in *Proceedings of the IEEE conference on Computer Vision and Pattern Recognition*, 2018, pp. 3569–3577.
- [34] S. Casas, W. Luo, and R. Urtasun, "Intentnet: Learning to predict intention from raw sensor data," in *Conference on Robot Learning*. PMLR, 2018, pp. 947–956.
- [35] C. Luo, X. Yang, and A. Yuille, "Self-Supervised Pillar Motion Learning for Autonomous Driving," *Proceedings of the IEEE Computer Society Conference on Computer Vision and Pattern Recognition*, pp. 3182–3191, 2021.
- [36] A. K. Akan and F. Güney, "Stretchbev: Stretching future instance prediction spatially and temporally," *arXiv preprint arXiv:2203.13641*, 2022.
- [37] S. Hu, L. Chen, P. Wu, H. Li, J. Yan, and D. Tao, "St-p3: End-to-end vision-based autonomous driving via spatial-temporal feature learning," *arXiv preprint arXiv:2207.07601*, 2022.
- [38] Y. Zhang, Z. Zhu, W. Zheng, J. Huang, G. Huang, J. Zhou, and J. Lu, "Beverse: Unified perception and prediction in birds-eye-view for vision-centric autonomous driving," *arXiv preprint arXiv:2205.09743*, 2022.
- [39] J. Philbin and S. Fidler, "Lift, Splat, Shoot: Encoding Images from Arbitrary Camera Rigs by Implicitly Unprojecting to 3D," *Lecture Notes*

- in *Computer Science (including subseries Lecture Notes in Artificial Intelligence and Lecture Notes in Bioinformatics)*, vol. 12359 LNCS, pp. 194–210, 2020.
- [40] A. H. Lang, S. Vora, H. Caesar, L. Zhou, J. Yang, and O. Beijbom, “Pointpillars: Fast encoders for object detection from point clouds,” in *Proceedings of the IEEE/CVF conference on computer vision and pattern recognition*, 2019, pp. 12 697–12 705.
 - [41] Y. H. Khalil and H. T. Mouftah, “Licanet: Further enhancement of joint perception and motion prediction based on multi-modal fusion,” *IEEE Open Journal of Intelligent Transportation Systems*, vol. 3, pp. 222–235, 2022.
 - [42] —, “Licanext: Incorporating sequential range residuals for additional advancement in joint perception and motion prediction,” *IEEE Access*, vol. 9, pp. 146 244–146 255, 2021.
 - [43] T. Cortinhal, G. Tzelepis, and E. Erdal Aksoy, “Salsanext: Fast, uncertainty-aware semantic segmentation of lidar point clouds,” in *Advances in Visual Computing*, G. Bebis, Z. Yin, E. Kim, J. Bender, K. Subr, B. C. Kwon, J. Zhao, D. Kalkofen, and G. Baciu, Eds. Cham: Springer International Publishing, 2020, pp. 207–222.
 - [44] E. De Brouwer, J. Simm, A. Arany, and Y. Moreau, “Grude-bayes: Continuous modeling of sporadically-observed time series,” in *Advances in Neural Information Processing Systems*, H. Wallach, H. Larochelle, A. Beygelzimer, F. d’Alché-Buc, E. Fox, and R. Garnett, Eds., vol. 32. Curran Associates, Inc., 2019. [Online]. Available: <https://proceedings.neurips.cc/paper/2019/file/455cb2657aaa59e32fad80cb0b65b9dc-Paper.pdf>
 - [45] H. Caesar, V. Bankiti, A. H. Lang, S. Vora, V. E. Liong, Q. Xu, A. Krishnan, Y. Pan, G. Baldan, and O. Beijbom, “nuscenes: A multimodal dataset for autonomous driving,” in *2020 IEEE/CVF Conference on Computer Vision and Pattern Recognition (CVPR)*, 2020, pp. 11 618–11 628.
 - [46] R. Kesten, M. Usman, J. Houston, T. Pandya, K. Nadhamuni, A. Ferreira, M. Yuan, B. Low, A. Jain, P. Ondruska, S. Omari, S. Shah, A. Kulkarni, A. Kazakova, C. Tao, L. Platinsky, W. Jiang, and V. Shet, “Level 5 perception dataset 2020,” <https://level-5.global/level5/data/>, 2019.
 - [47] D. Kim, S. Woo, J.-Y. Lee, and I. S. Kweon, “Video panoptic segmentation,” in *2020 IEEE/CVF Conference on Computer Vision and Pattern Recognition (CVPR)*, 2020, pp. 9856–9865.
 - [48] M. Tan and Q. Le, “Efficientnet: Rethinking model scaling for convolutional neural networks,” in *International conference on machine learning*. PMLR, 2019, pp. 6105–6114.
 - [49] Z. Liu, Y. Lin, Y. Cao, H. Hu, Y. Wei, Z. Zhang, S. Lin, and B. Guo, “Swin transformer: Hierarchical vision transformer using shifted windows,” in *Proceedings of the IEEE/CVF international conference on computer vision*, 2021, pp. 10 012–10 022.
 - [50] C. Lu, M. J. G. van de Molengraft, and G. Dubbelman, “Monocular Semantic Occupancy Grid Mapping With Convolutional Variational Encoder–Decoder Networks,” *IEEE Robotics and Automation Letters*, vol. 4, no. 2, pp. 445–452, 2019.
 - [51] B. Pan, J. Sun, H. Y. T. Leung, A. Andonian, and B. Zhou, “Cross-view semantic segmentation for sensing surroundings,” *IEEE Robotics and Automation Letters*, vol. 5, no. 3, pp. 4867–4873, 2020.
 - [52] T. Roddick and R. Cipolla, “Predicting semantic map representations from images using pyramid occupancy networks,” in *2020 IEEE/CVF Conference on Computer Vision and Pattern Recognition (CVPR)*, 2020, pp. 11 135–11 144.
 - [53] H. Wang, P. Cai, Y. Sun, L. Wang, and M. Liu, “Learning interpretable end-to-end vision-based motion planning for autonomous driving with optical flow distillation,” in *2021 IEEE International Conference on Robotics and Automation (ICRA)*. IEEE, 2021, pp. 13 731–13 737.